Electronic Supplementary Material (ESI) for Soft Matter.


# Electronic Supplementary Information to: Combining adhesive contact mechanics with a viscoelastic material model to probe local material properties by AFM

Christian Ganser[a,b,*], Caterina Czibula[a,b], Daniel Tscharnuter[c], Thomas Schöberl[d], Christian Teichert[a,b], and Ulrich Hirn[b,e]

[a]Institute of Physics, Montanuniversitaet Leoben, Franz Josef - Str. 18, 8700 Leoben, Austria.*E-mail: christian.ganser@alumni.unileoben.ac.at
[b]Christian Doppler Laboratory for Fiber Swelling and Paper Performance, Graz University of Technology, Inffeldgasse 23, 8010 Graz, Austria.
[c]Polymer Competence Center Leoben GmbH, Roseggerstr. 12, 8700 Leoben, Austria.
[d]Erich Schmid Institute, Jahnstr. 12, 8700 Leoben, Austria.
[e]Institute of Paper, Pulp and Fiber Technology, Graz University of Technology, Inffeldgasse 23, 8010 Graz, Austria.

In section 1, the calculation of stress $\sigma$ and strain $\varepsilon$ under an indenting tip is presented, by utilizing the JKR theory. Then, in sections 2 and 3, in order to facilitate the use of our model and procedure presented in the main text, the GNU/Octave representations of the combination of the JKR model with the SLS (section 2) and GM2 model (section 3) are shown. Both code snippets below can be used directly to calculate the indentation depth as a function of time with the GNU/Octave's `lsode` function. Section 4 provides an overview of the parameters and variables used for the described method. In section 5, the influence of the adhesion force to the results is studied, whereas in section 6 the sensitivity of the model to the initial parameters is investigated. Representative force vs. indentation depth plots are provided in section 7 for both the determination of reduced modulus and hardness as well as viscoelastic parameters.

## 1 Calculating the stress and strain under the indenter

The JKR theory describes the contact radius $a$ as a function of the force $F$ by[1]

$$a^3 = \frac{3R}{4E}\widetilde{F}, \tag{1}$$

with

$$\widetilde{F} = F + 2F_{ad} + 2\left(F_{ad}F + F_{ad}^2\right)^{\frac{1}{2}}. \tag{2}$$

The relationship between $a$ and indentation depth $\delta$ is given by[2,3]

$$\delta = \frac{a^2}{R} - \left(\frac{4aF_{ad}}{3RE}\right)^{\frac{1}{2}}. \tag{3}$$

From equation 1 the reduced modulus $E$ can be expressed as

$$E = \frac{3R}{4a^3}\widetilde{F} \tag{4}$$

and inserted in equation 3 to get

$$\delta = \frac{a^2}{R}\left[1 - \frac{4}{3}\left(\frac{F_{ad}}{\widetilde{F}}\right)^{\frac{1}{2}}\right]. \tag{5}$$

Equation 5 can then be used to express the contact radius $a$ in terms of the measureable quantities $R$, $\delta$, $F$, and $F_{ad}$:

$$a^2 = \frac{R\delta}{1 - \frac{4}{3}\left(\frac{F_{ad}}{\widetilde{F}}\right)^{\frac{1}{2}}}. \tag{6}$$

Now, the stress beneath the indenter has to be calcuated. The theory gives the following stress distribution for a spherical indenter where $r$ is the lateral coordinate, with $r = 0$ describing the center of the circular contact area and $r = a$ its rim:[3]

$$\sigma(r) = \frac{E}{\pi}\left(\frac{\delta}{a} - \frac{a}{R}\right)\left(1 - \frac{r^2}{a^2}\right)^{-\frac{1}{2}} + \frac{2Ea}{\pi R}\left(1 - \frac{r^2}{a^2}\right)^{\frac{1}{2}}. \tag{7}$$

Then, the stress is averaged over the contact region with contact radius $a$ by

$$\sigma_{JKR} = \frac{1}{a}\int_{r=0}^{a} \sigma(r)dr = \frac{E\delta}{2a}. \tag{8}$$

Inserting equation 4 in equation 8 gives

$$\sigma_{JKR} = \frac{3R\delta}{8a^4}\widetilde{F} \tag{9}$$

and the contact radius $a$ can be eliminated by inserting equation 6 in equation 9, which yields

$$\sigma_{JKR} = \frac{3\widetilde{F}}{8R\delta}\left[1 - \frac{4}{3}\left(\frac{F_{ad}}{\widetilde{F}}\right)^{\frac{1}{2}}\right]^2. \tag{10}$$

In this article, the stress beneath the indenter $\sigma_{JKR}$ is calculated using equation 10, as is stated in the main text.

Now, only the strain $\varepsilon_{JKR}$ remains unknown. Here, it will be assumed that Hooke's law is valid for the average stress $\sigma_{JKR}$ and average strain $\varepsilon_{JKR}$

$$\varepsilon_{JKR} = \sigma_{JKR}E^{-1}. \tag{11}$$

By inserting equation 8 in equation 11, $\sigma_{JKR}$ and $E$ are eliminated and only

$$\varepsilon_{JKR} = \frac{1}{2}\frac{\delta}{a} \tag{12}$$

remains. Now, $a$ in equation 12 is eliminated by inserting equation 6, which yields

$$\varepsilon_{JKR} = \frac{1}{2}\left(\frac{\delta}{R}\right)^{\frac{1}{2}}\left[1 - \frac{4}{3}\left(\frac{F_{ad}}{\widetilde{F}}\right)^{\frac{1}{2}}\right]^{\frac{1}{2}}. \tag{13}$$

This equation is identical to the one given in the main text to describe the average strain beneath the indenter.

Equation 11 is a usual assumption for the linear elastic regime and commonly used to calculate strain in contact mechanics.[4–7] Note that in the cited works, the stress and strain terms are not identical to the ones used here as adhesion is not considered. However, even when comparing our stress and strain definitions at zero adhesion force (identical to the Hertz model) it turns out that in the case of the common nanoindentation stress and strain,[5] they differ by a constant factor: $\sigma_{JKR} = c_1\sigma_{NI}$ and $\varepsilon_{JKR} = c_2\varepsilon_{NI}$. $c_1$ and $c_2$ are the constant factors and the index $NI$ identifies the nanoindentation stress and strain definitions found in the literature. The resulting modulus also differs by a constant factor, so that $E = c_1 c_2^{-1} c_3 E_{NI}$. In the case of nanoindentation stress and strain $c_1 = 3\pi/8$, $c_2 = 1/2$, and $c_3 = 4/(3\pi)$ so that $c_1 c_2^{-1} c_3 = 1$. This means that while stress and strain differ by a constant factor, the modulus definitions are identical.

## 2 Standard linear solid (SLS) model

In the following code, which represents the differential equation for the indentation depth by using the SLS model to describe the time dependent material behavior, the variables are:

| | | | |
|---|---|---|---|
| E_1 | ... | $E_\infty$ | |
| E_2 | ... | $E_1$ | |
| eta | ... | $\eta$ | |
| F | ... | $F$ | force schedule $F(t)$ |
| dFdt | ... | $\frac{dF}{dt}$ | time derivative of the force schedule $\frac{dF}{dt}(t)$ |
| R | ... | $R$ | tip radius or effective radius |
| F_ad | ... | $F_{ad}$ | adhesion force |
| y | ... | $\delta$ | indentation depth |
| dy | ... | $\frac{d\delta}{dt}$ | time derivative of the indentation depth |

```
A = E_1;
B = eta*((E_1 + E_2)./E_2);
C = eta./E_2;

F_twiddle = F + 2*F_ad + 2*(F_ad*F + F_ad^2)^(1/2);
F_twiddle_dot = dFdt*(1 + F_ad*(F_ad*(F_ad + F))^(-1/2));

dy = (y*(sqrt(-((R*y)/(-3+4*sqrt(F_ad/F_twiddle))))*F_twiddle ...
*(-16*F_ad+3*(-3+8*sqrt(F_ad/F_twiddle))*F_twiddle+3*C*(-3+4 ...
*sqrt(F_ad/F_twiddle))*F_twiddle_dot)+4*sqrt(3)*R*y^2*(A*F_twiddle ...
-(B*sqrt(F_ad/F_twiddle)*F_twiddle_dot)/(-3+4*sqrt(F_ad ...
/F_twiddle)))))/(F_twiddle*(-2*sqrt(3)*B*R*y^2+C*sqrt(-((R*y)/(-3 ...
+4*sqrt(F_ad/F_twiddle))))*(-16*F_ad+3*(-3 ...
+8*sqrt(F_ad/F_twiddle))*F_twiddle)));
```

## 3 Generalized Maxwell order 2 (GM2) model

The constitutive equation for the GM2 model is a second order differential equation of the following form

$$\sigma = A\varepsilon + B\dot{\varepsilon} + C\ddot{\varepsilon} - D\dot{\sigma} - E\ddot{\sigma},$$

with

$$A = E_1$$

$$B = \left( \frac{\eta_1 + \eta_2}{E_\infty} + \frac{\eta_1}{E_1} + \frac{\eta_2}{E_2} \right) E_\infty$$

$$C = \frac{\eta_1 \eta_2}{E_1 E_2} (E_\infty + E_1 + E_2)$$

$$D = \frac{\eta_1}{E_1} + \frac{\eta_2}{E_2}$$

$$E = \frac{\eta_1 \eta_2}{E_1 E_2}.$$

To solve this second order differential equation numerically, it has to be written as a system of two differential equations of first order, as is done below. The variables used have the following meaning:

| | | | |
|---|---|---|---|
| E_1 | ... | $E_\infty$ | |
| E_2 | ... | $E_1$ | |
| E_3 | ... | $E_2$ | |
| eta | ... | $\eta_1$ | |
| eta2 | ... | $\eta_2$ | |
| F | ... | $F$ | force schedule $F(t)$ |
| dFdt | ... | $\frac{dF}{dt}$ | time derivative of the force schedule $\frac{dF}{dt}(t)$ |
| d2Fdt2 | ... | $\frac{d^2F}{dt^2}$ | second time derivative of the force schedule $\frac{d^2F}{dt^2}(t)$ |
| R | ... | $R$ | tip radius or effective radius |
| F_ad | ... | $F_{ad}$ | adhesion force |
| y(1) | ... | $\delta$ | indentation depth |
| y(2) | ... | $\frac{d\delta}{dt}$ | time derivative of the indentation depth |
| dy(1) | ... | $\frac{d\delta}{dt}$ | time derivative of the indentation depth |
| dy(2) | ... | $\frac{d^2\delta}{dt^2}$ | second time derivative of the indentation depth |

```
A = E_1;
B = ((eta + eta2)/E_1 + eta/E_2 + eta2/E_3)*E_1;
C = (eta*eta2/(E_2*E_3))*(E_1 + E_2 + E_3);
D = (eta/E_2 + eta2/E_3);
E = eta*eta2/(E_2*E_3);

F_twiddle = F + 2*F_ad + 2*(F_ad*F + F_ad^2)^(1/2);
F_twiddle_dot = (1 + F_ad/sqrt(F_ad*(F_ad + F)))*dFdt;
F_twiddle_2dot = d2Fdt2 + (sqrt(F_ad)*(-dFdt^2 + 2*(F_ad ...
+ F)*d2Fdt2))/(2*(F_ad + F)^(3/2));

dy(1) = y(2);

dy(2) = (y(1)^2*sqrt((R*y(1))/(3-4*sqrt(F_ad/F_twiddle))) ...
*(-3+4*sqrt(F_ad/F_twiddle))^3*F_twiddle*(-((2*E*(16 ...
*F_ad+(9-24*sqrt(F_ad/F_twiddle))*F_twiddle)*y(2)^2) ...
/y(1)^3)+(y(2)*(3*D*(3-8*sqrt(F_ad/F_twiddle))*F_twiddle ...
+sqrt(3)*C*sqrt((R*y(1))/(3-4*sqrt(F_ad/F_twiddle)))*(-3 ...
+4*sqrt(F_ad/F_twiddle))*y(2)+2*(8*D*F_ad+3*E*(3-4 ...
*sqrt(F_ad/F_twiddle))*F_twiddle_dot)))/y(1)^2+(1/((3-4 ...
*sqrt(F_ad/F_twiddle))^2*F_twiddle^3))*2*sqrt(3) ...
*sqrt((R*y(1))/(3-4*sqrt(F_ad/F_twiddle)))*(54*A*(1 ...
-4*sqrt(F_ad/F_twiddle))*F_twiddle^3+2*C*F_ad*(33 ...
-20*sqrt(F_ad/F_twiddle))*F_twiddle_dot^2+F_twiddle ...
*(16*B*F_ad*(-3+2*sqrt(F_ad/F_twiddle))*F_twiddle_dot ...
-27*C*sqrt(F_ad/F_twiddle)*F_twiddle_dot^2+16*C*F_ad ...
*(-3+2*sqrt(F_ad/F_twiddle))*F_twiddle_2dot)+2 ...
*F_twiddle^2*(16*A*F_ad*(9-4*sqrt(F_ad/F_twiddle)) ...
+9*sqrt(F_ad/F_twiddle)*(B*F_twiddle_dot ...
+C*F_twiddle_2dot)))+(1/(y(1)*F_twiddle))*(3*(-3 ...
+8*sqrt(F_ad/F_twiddle))*F_twiddle^2 ...
+2*sqrt(F_ad/F_twiddle)*F_twiddle_dot*(2*sqrt(3)*C ...
*sqrt((R*y(1))/(3-4*sqrt(F_ad/F_twiddle)))*y(2) ...
-3*E*F_twiddle_dot)+F_twiddle*(-16*F_ad+(2*B*R ...
*y(1)*y(2))/sqrt((R*y(1))/(9-12*sqrt(F_ad/F_twiddle))) ...
-9*D*F_twiddle_dot-9*E*F_twiddle_2dot+12 ...
*sqrt(F_ad/F_twiddle)*(D*F_twiddle_dot ...
+E*F_twiddle_2dot)))))/(2*sqrt(3)*C*R*y(1)^2*(16 ...
```

```
*F_ad*(9-4*sqrt(F_ad/F_twiddle))+27*(1 ...
-4*sqrt(F_ad/F_twiddle))*F_twiddle)+E*sqrt((R*y(1)) ...
/(3-4*sqrt(F_ad/F_twiddle)))*(256*F_ad^2*(15 ...
-4*sqrt(F_ad/F_twiddle))+1440*F_ad*(3 ...
-4*sqrt(F_ad/F_twiddle))*F_twiddle+81*(3 ...
-20*sqrt(F_ad/F_twiddle))*F_twiddle^2));
```

# 4 Parameter Summary

In this section, we provide a short summary of the parameters and quantities that are measured (input) and those that are determined from fitting the constitutive equation in $\delta$ and $F$ (given as GNU/Octave code above) to the experiment (output).

**measured constants** (input)

| | | |
|---|---|---|
| $R_{tip}$ | ... | by tip characterizer |
| $F_{ad}$ | ... | during retraction from the surface at the end of the experiment |
| $\delta_{plast}$ | ... | residual indentation depth after plastic deformation |
| $\delta_{max}$ | ... | maximum indentation depth during plastic deformation |
| $\delta_0$ | ... | difference in indentation between contact and elastic pre-loading |

**measured quantities, time resolved** (input)

| | | |
|---|---|---|
| $\delta(t)$ | ... | by monitoring the AFM's piezo elongation and cantilever deflection |
| $F(t)$ | ... | by AFM cantilever deflection (only for verification) |

**assumed parameters** (input)

| | | |
|---|---|---|
| $\nu$ | ... | $\nu^2 \ll 1 \Rightarrow (1-\nu^2)/E \approx 1/E$ in eq. 1 |
| $\dot{\delta}_0$ | ... | 0 |

**parameters determined by fitting the model to the experiment** (output)

$E_\infty$, $E_1$, $E_2$, $\eta_1$, $\eta_2$

# 5 Influence of adhesion force

In this section, the influence of the adhesion force $F_{ad}$ to the creep curves $\delta(t)$ is studied and the error that is made by neglecting the adhesion force is investigated. First only calculated creep curves are considered and then it is shown that also the parameters determined from experimental data suffer from neglecting the adhesion force.

## 5.1 General effects of adhesion

First, the effect of the adhesion force to the creep curve $\delta(t)$ is displayed in figure S1. The curves were calculated using the GM2 model in combination with the JKR model (for $F_{ad} > 0$) and Hertz model (for $F_{ad} = 0$). The parameters were: $E_\infty = 2.3\,\text{GPa}$, $E_1 = 1.5\,\text{GPa}$, $E_2 = 0.8\,\text{GPa}$, $\eta_1 = 1.3\,\text{GPa s}$, $\eta_2 = 13\,\text{GPa s}$, $R_{tip} = 350\,\text{nm}$, $R_i = 2R_{tip}$, $F_0 = 50\,\text{nN}$, $\dot{\delta}_0 = 0$. $\delta_0$ was determined from the JKR contact mechanics for $E = E_\infty$ (which is consistent with $\dot{\delta}_0 = 0$). The load schedule was identical to the one used in the experiments. The adhesion force is varied from 0 to 300 nN in steps of 100 nN.

In the magnification of the initial creep curve (figure S1b), it can be seen that the initial indentation depth is increasing with increasing adhesion force. The overall curve (figure S1a) shows that also the final indentation depth (at $t = 120\,\text{s}$) is increasing with increasing adhesion force. Both observations make sense, as an increase in adhesion force is an effective increase of the overall acting force and, thus, the indentation depth should increase if the adhesion force increases and the mechanical parameters stay constant.

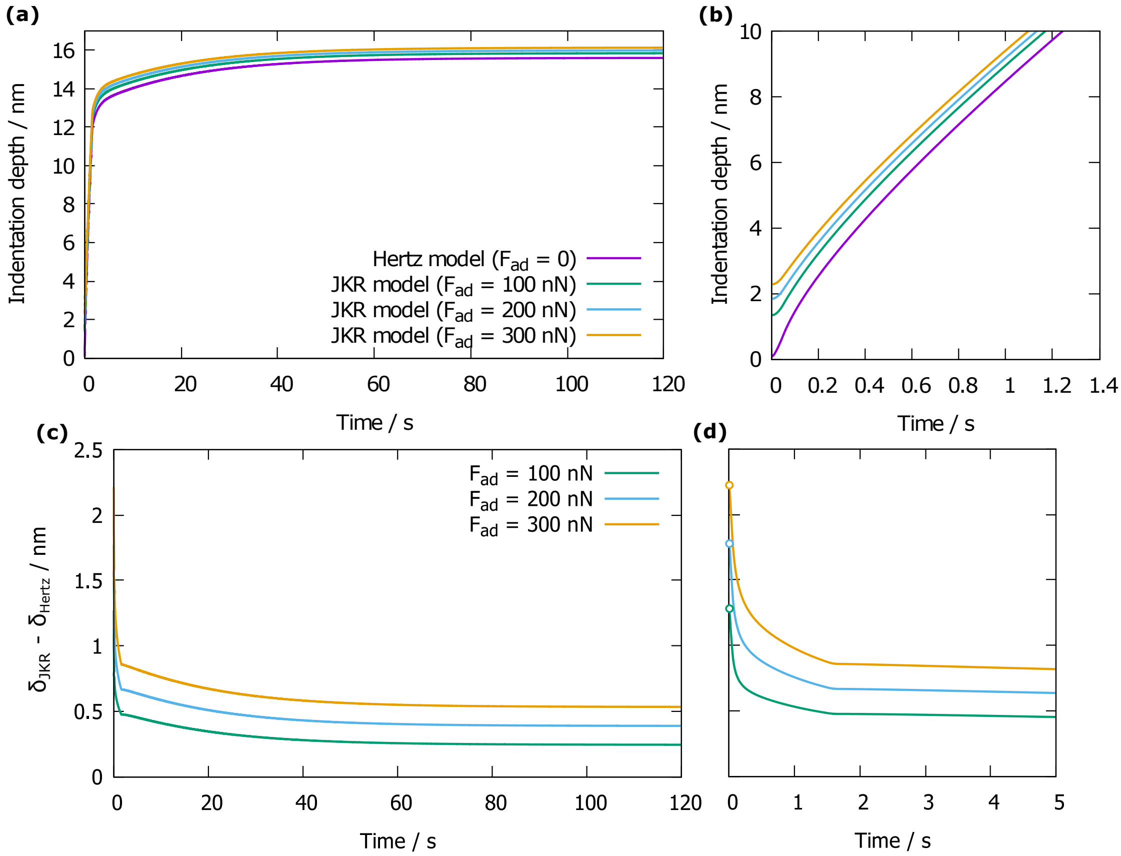


Figure S1: The influence of adhesion force to the indentation depth. The curves were calculated using the GM2 model in combination with the JKR or Hertz model, as indicated. (a) full curves, (b) the first 1.4 s of (a), (c) difference between JKR indentation depth ($\delta_{JKR}$) and the Hertz indentation depth ($\delta_{Hertz}$), (d) the first 5 s of (c).

The difference between the curve without adhesion and the ones with adhesion is plotted in figure S1c and S1d. At $t = 0$ s the difference is relatively large (e.g. 2.2 nm for $F_{ad} = 300$ nN) and decreases during the loading segment quickly (at $t = 120$ s it is about 0.53 nm for $F_{ad} = 300$ nN) to become approximately constant from $t \approx 80$ s. This means that the influence of the adhesion force is decreasing with increasing indentation depth, but it does not appear to vanish completely.

## 5.2 Neglecting adhesion: simulated data

Now, what happens when the adhesion force is neglected and a curve calculated with $F_{ad}$ = 300 nN and other parameters as specified above is fitted with the Hertz model? Note that there are two possibilities to do this. One is that the calculated JKR curve is not changed and left with the initial conditions (IC) corresponding to the JKR model ($\delta_0 \neq 0$ if $F_{ad} \neq 0$ and $F \geq 0$). The other possibility is to shift the JKR curve, so that the initial condition of the Hertz model is satisfied ($\delta_0 = 0$ if $F = 0$). The results of fitting a calculated creep curve (using the JKR-GM2 model) with the Hertz model using both possibilities are presented in table S1.

The first case, using the JKR initial conditions for the Hertz model, is inconsistent with the Hertz theory as it would imply a pre-existing deformation without an external force. This is evident from the resulting fit parameters, shown in the second column of table S1. They are clearly different from the parameters that were used to calculate the

Table S1: Comparison of parameters; original: used as an input to the JKR-GM2 model; JKR IC: from fitting with a Hertz-GM2 model using the JKR IC; Hertz IC: from fitting with a Hertz-GM2 model by using the Hertz IC and offsetting the data; see the text for other parameters used

| | original | JKR IC | Hertz IC |
|---|---|---|---|
| $E_\infty$ / GPa | 2.3 | 2.2 | 2.8 |
| $E_1$ / GPa | 1.5 | 3.7 | 0.007 |
| $E_2$ / GPa | 0.8 | 2.2 | 0.18 |
| $\eta_1$ / GPa s | 1.3 | 2.0 | 0.004 |
| $\eta_2$ / GPa s | 13 | 29 | 2.8 |

curve using the JKR model as specified in the first column of table S1. The resulting fit and the original data are plotted in figure S2. Although the model is clearly wrong (the original data is calculated with the JKR model but fitted with the Hertz model) and produces incorrect parameters, the fit converged and seems to describe the data well. The main problem with this approach is that adhesion is partially acknowledged, by supplying an initial deformation but not the force needed to create it, without a proper framework to handle such conditions.

The second case, using the Hertz initial conditions by offsetting the data, is also problematic as we completely neglect the deformation caused by adhesion. However, it is consistent with the applied model. In this case, however, fits did not converge with the initial parameter $\dot{\delta}_0 = 0$. It was possible to fit the data only when the initial creep rate $\dot{\delta}_0$ was raised to $0.1\,\mathrm{nm\,s^{-1}}$. Again, this is inconsistent with the actual initial conditions during calculation of data to be fitted. As one would expect, also in this case the determined parameters were different from the parameters used to generate the curve (compare the third column of table S1 with the first column). In this case, the fit seems to deviate slightly from the JKR model at $t < 5\,\mathrm{s}$ (see figure S2b).

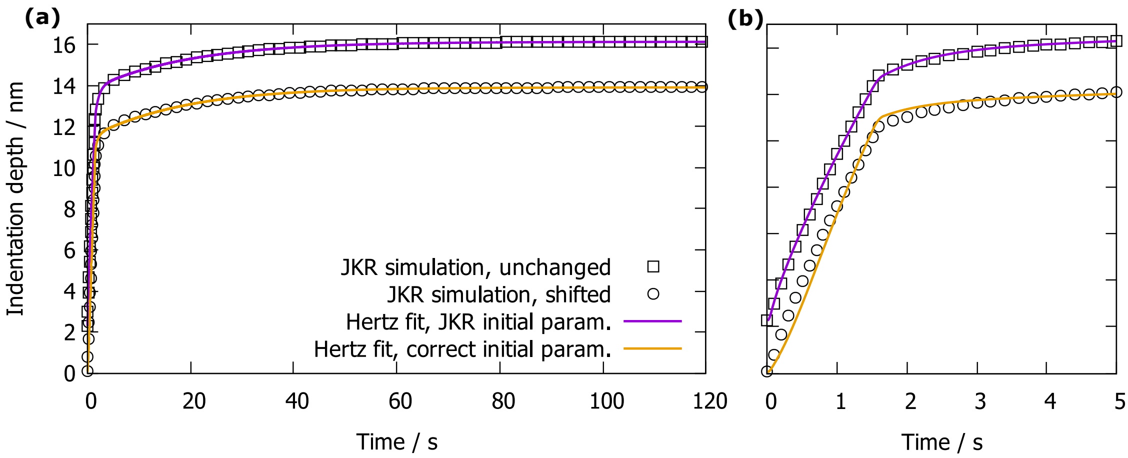


Figure S2: Curves simulated with the JKR model (squares and circles) and the corresponding fits using the Hertz model. Squares indicate a fit using JKR initial conditions. Circles describe the JKR curve that has been shifted to meet the Hertz initial conditions. (a) full curves, (b) the first 5 s of (a).

If the adhesion force is small, e.g. 30 nN, neglecting it becomes less of a problem. If such a creep curve (calculated with JKR-GM2, $F_{ad} = 30\,\mathrm{nN}$, other parameters same as before) is fitted with a Hertz-GM2 model, the resulting viscoelastic parameters are (relative deviations from the values used as input for the JKR model are given in brackets): $E_\infty = 2.3\,\mathrm{GPa}$ (+0%), $E_1 = 2.1\,\mathrm{GPa}$ (+40%), $E_2 = 1.1\,\mathrm{GPa}$ (+38%), $\eta_1 = 1.5\,\mathrm{GPa\,s}$ (+15%), $\eta_2 = 17\,\mathrm{GPa\,s}$ (+31%). Interestingly, offsetting the data to suit the Hertz initial conditions did still not work because also in this case the fit did not converge for $\dot{\delta_0} = 0$.

### 5.3 Neglecting adhesion: experimental data

Here, it is demonstrated what happens when adhesion is neglected when evaluating experimental data. Only the curves that have been averaged from single curves on one position are fitted to reduce the scattering, as is described in the main text. Again both cases (Hertz model with JKR initial conditions and Hertz model with Hertz initial conditions) are investigated. Similarly to the simulated data, it was not possible to fit the experimental data using the Hertz initial conditions and $\dot{\delta_0} = 0$. In fact, $\dot{\delta_0}$ had to varied between $0.1\,\mathrm{nm\,s^{-1}}$ and $0.5\,\mathrm{nm\,s^{-1}}$ to be able to fit the data. This fact alone renders the parameters obtained untrustworthy. Fitting the experiments with the Hertz model and the JKR initial conditions worked well without the need to adjust $\dot{\delta_0}$, or anything else. The parameters obtained by the Hertz model are compared to the parameters obtained by the JKR model (the ones presented and discussed in the main text) in table S2.

Table S2: Viscoelastic parameters obtained by fitting the experimental data with a GM2 model in combination with JKR contact mechanics and compared to parameters obtained from combining a GM2 model with Hertz contact mechanics using JKR IC as well as Hertz IC

| | JKR | Hertz (JKR IC) | Hertz (Hertz IC) |
|---|---|---|---|
| | | PC | |
| $E_\infty$ / GPa | $1.52 \pm 0.18$ | $1.43 \pm 0.18$ | $1.99 \pm 0.31$ |
| $E_1$ / GPa | $1.62 \pm 0.84$ | $4.93 \pm 2.59$ | $0.80 \pm 0.64$ |
| $E_2$ / GPa | $0.62 \pm 0.21$ | $1.43 \pm 0.49$ | $0.56 \pm 0.32$ |
| $\eta_1$ / GPa s | $0.52 \pm 0.22$ | $0.85 \pm 0.31$ | $0.62 \pm 0.24$ |
| $\eta_2$ / GPa s | $7.2 \pm 4.2$ | $13.5 \pm 5.8$ | $7.2 \pm 3.9$ |
| | | PMMA | |
| $E_\infty$ / GPa | $2.33 \pm 0.26$ | $2.23 \pm 0.25$ | $3.14 \pm 0.36$ |
| $E_1$ / GPa | $1.51 \pm 0.71$ | $4.16 \pm 2.51$ | $0.74 \pm 0.67$ |
| $E_2$ / GPa | $0.81 \pm 0.35$ | $2.08 \pm 0.76$ | $1.42 \pm 0.97$ |
| $\eta_1$ / GPa s | $1.31 \pm 1.22$ | $1.76 \pm 1.42$ | $0.83 \pm 0.67$ |
| $\eta_2$ / GPa s | $12.7 \pm 6.8$ | $31.5 \pm 24.8$ | $17.2 \pm 11.6$ |

The parameters obtained by fitting the experimental data with the Hertz-GM2 model by using the JKR initial conditions (table S2, column two), show the exact same behavior as was observed for the simulated data: $E_\infty$ is slightly decreased compared to the JKR model, $E_1$ is strongly increased, $E_2$ is increased, $\eta_1$ is about the same, and $\eta_2$ is again strongly increased. This leads to the conclusion that in this evaluation adhesion cannot be neglected.

By fitting the data with the Hertz model using the Hertz initial conditions (table S2, column three), $E_\infty$ becomes significantly higher compared to the values obtained by the JKR model. All values do seem plausible and for PC the results are closer to results obtained by NI (see main text). However, as mentioned above, the initial creep rate $\dot{\delta_0}$ had to be adjusted significantly for the fit to converge for the GM2-Hertz model using the Hertz initial conditions. This behavior is completely consistent with the behavior observed for simulated data (see section 5.2), where it is directly visible that parameters obtained this way are incorrect. Thus, adhesion cannot be neglected.

### 5.4 Neglecting adhesion: conclusion

From the investigations in this section, it becomes clear that even when the maximum force used is 5000 nN an adhesion force of 300 nN cannot be neglected. Even an adhesion force as low as 30 nN would yield parameters that are off by as much as 40%. Interestingly, it was never possible to fit the simulated data properly with the Hertz model and using the Hertz initial conditions. Basically, this means that the effect of adhesion has to be acknowledged (albeit the adhesion being low) in the initial parameters to gain useful results.

## 6 Sensitivity to input parameters

Here, the influence of slightly deviating input parameters on the determined viscoelastic parameters is studied. For this purpose, a creep curve is calculated using the JKR+GM2 model. This creep curve is then treated like experimental data and fitted with the JKR+GM2 model, as described in the main text. However, one input parameter is changed slightly from the correct value that was used to calculate the curve. The parameters used to generate this curve were: $E_\infty = 2.3\,\mathrm{GPa}$, $E_1 = 1.5\,\mathrm{GPa}$, $E_2 = 0.8\,\mathrm{GPa}$, $\eta_1 = 1.3\,\mathrm{GPa\,s}$, $\eta_2 = 13\,\mathrm{GPa\,s}$, $R_{tip} = 350\,\mathrm{nm}$, $R_i = 2R_{tip}$, $F_{ad} = 300\,\mathrm{nN}$. Parameters that are changed from the ones stated here are indicated in the text below.

### 6.1 Adhesion force

The adhesion force is a parameter that is measured during the experiment and is, thus, subject to some uncertainty. To check the sensitivity of the model to a deviating $F_{ad}$, three creep curves with respective adhesion forces of 100 nN, 200 nN, and 300 nN were generated. Other parameters were as stated above. For evaluating the calculated curves, the adhesion force is changed by ±10%. The results are presented in table S3. If the adhesion force is assumed to be off by 10% during evaluation, the resulting parameters are off by < 10% in the investigated range. The parameter that exhibits the largest relative deviation is $E_2$ with about 9% at $F_{ad} = 300\,\mathrm{nN}$. Increasing the deviation of $F_{ad}$ to 20%, increases the deviations in the resulting parameters about twofold compared to the 10% case. While the level of the adhesion force does have an influence on the deviation in the parameters, it is very low, as can be seen from table S3.

Table S3: Sensitivity of the JKR+GM2 model to the fit input parameter $F_{ad}$

| $F_{ad}$ (correct) / nN | | 300 | | | 200 | | | 100 | |
|---|---|---|---|---|---|---|---|---|---|
| $F_{ad}$ (fit) / nN | 300 | 270 | 330 | 200 | 180 | 220 | 100 | 90 | 110 |
| $E_\infty$ / GPa | 2.30 | 2.29 | 2.31 | 2.30 | 2.29 | 2.31 | 2.30 | 2.30 | 2.30 |
| $E_1$ / GPa | 1.50 | 1.52 | 1.47 | 1.50 | 1.53 | 1.47 | 1.50 | 1.53 | 1.47 |
| $E_2$ / GPa | 0.80 | 0.87 | 0.73 | 0.80 | 0.86 | 0.74 | 0.80 | 0.84 | 0.76 |
| $\eta_1$ / GPa s | 1.30 | 1.31 | 1.29 | 1.30 | 1.31 | 1.29 | 1.30 | 1.31 | 1.29 |
| $\eta_2$ / GPa s | 13.0 | 14.0 | 12.0 | 13.0 | 13.8 | 12.2 | 13.0 | 13.6 | 12.4 |

### 6.2 Initial parameter $\delta_0$

Another parameter that is determined from measurements is the initial parameter $\delta(t = 0) = \delta_0$, which is necessary for numerically solving a differential equation of order $\geq 1$. One curve was calculated to study the sensitivity to $\delta_0$, using the parameters exactly as stated above. The correct value for $\delta_0$ is determined using the JKR theory with $F = F_0 = 50\,nN$ and $E_\infty$ as the modulus, which is consistent with the assumption $\dot{\delta}(t = 0) = 0$. This generated curve is then treated as experimental data and fitted with the JKR+GM2 model described in the main text. The input parameter $\delta_0$ is varied by ± 10%, ± 20%, and

$\pm 30\%$, other input parameters are kept at the correct value. The results are presented in table S4.

Table S4: Sensitivity of the JKR+GM2 model to the fit input parameter $\delta_0$

| $\delta_0$ (fit) / nm | 1.60 | 1.82 | 2.05 | 2.28 | 2.51 | 2.74 | 2.96 |
|---|---|---|---|---|---|---|---|
| | -30% | -20% | -10% | ±0% | +10% | +20% | +30% |
| $E_\infty$ / GPa | 2.45 | 2.40 | 2.35 | 2.30 | 2.25 | 2.21 | 2.16 |
| $E_1$ / GPa | 1.55 | 1.56 | 1.54 | 1.50 | 1.44 | 1.38 | 1.31 |
| $E_2$ / GPa | 0.38 | 0.55 | 0.69 | 0.80 | 0.89 | 0.97 | 1.03 |
| $\eta_1$ / GPa s | 1.34 | 1.33 | 1.32 | 1.30 | 1.28 | 1.25 | 1.22 |
| $\eta_2$ / GPa s | 6.46 | 9.27 | 11.4 | 13.0 | 14.3 | 15.3 | 16.2 |

The parameters that are affected the strongest by far are $E_2$ and $\eta_2$. Especially, underestimating $\delta_0$ leads to a large deviation in the aforementioned parameters. If $\delta_0$ is reduced by 30%, an increase of around 50% in $E_2$ and $\eta_2$ is found. On the other hand, if $\delta_0$ is increased by 30%, $E_2$ and $\eta_2$ only decrease by around 30%.

## 6.3 Initial parameter $\dot{\delta}(t = 0)$

The GM2 model results in a differential equation of order 2, thus, also $\dot{\delta}(t = 0)$ is needed as an initial parameter. It was, however, not possible to measure it reliably and was assumed to be 0, as is described in the main text. Here, 5 different creep curves are calculated with the parameters stated above, only $\dot{\delta}(t = 0)$ is changed, according to the first line in table S5. These five curves are then fitted by using $\dot{\delta}(t = 0) = 0$ as input.

Table S5: Sensitivity of the JKR+GM2 model to the fit input parameter $\dot{\delta}(t = 0)$; all values are determined by keeping $\dot{\delta}(t = 0) = 0$ during the fit; $\dot{\delta}(t = 0)$=0 of the curves to be fitted was set to the values given in the first line of the table

| $\dot{\delta}(t = 0)$ / nm s$^{-1}$ | -0.5 | -0.3 | -0.1 | 0 | 0.1 | 0.3 | 0.5 |
|---|---|---|---|---|---|---|---|
| $E_\infty$ / GPa | 2.30 | 2.30 | 2.30 | 2.30 | 2.30 | 2.30 | 2.30 |
| $E_1$ / GPa | 1.47 | 1.48 | 1.49 | 1.50 | 1.51 | 1.52 | 1.52 |
| $E_2$ / GPa | 1.16 | 1.01 | 0.87 | 0.80 | 0.73 | 0.60 | 0.47 |
| $\eta_1$ / GPa s | 1.22 | 1.26 | 1.29 | 1.30 | 1.31 | 1.34 | 1.35 |
| $\eta_2$ / GPa s | 18.1 | 16.1 | 14.0 | 13.0 | 12.0 | 9.96 | 7.94 |

$E_2$ and $\eta_2$ are affected the strongest when changing $\dot{\delta}(t = 0)$, similar to the other cases studied. For $\dot{\delta}(t = 0) = \pm 0.1\,\mathrm{nm\,s^{-1}}$, the parameters change by $< 10\%$.

## 6.4 Conclusions

Changing the adhesion force by a certain percentage led to a similar (slightly less) maximum relative change in the output parameters in the investigated range. Deviations in the initial indentation depth $\delta_0$ had a higher impact than deviations in the adhesion force. Especially, underestimating $\delta_0$ will considerably affect the output parameters. If an initial creep rate $\dot{\delta}(t = 0)$ of up to $0.1\,\mathrm{nm\,s^{-1}}$ is approximated by a creep rate of 0 in the evaluation, the output parameters are off by $< 10\%$. This should not be a problem, as creep rates $> 0.1\,\mathrm{nm\,s^{-1}}$ (i.e., a change in indentation depth that is larger then 1 nm per 10 s) is easily observable. It is interesting that the parameters that were affected the most were $E_2$ and $\eta_2$, by far. The other parameters changed in all the above investigations only by 7% at maximum. To conclude, the most important input parameter to determine is $\delta_0$, the initial indentation depth, followed by the adhesion force.

## 7 Force distance plots

In figure S3, force vs. indentation depth plots with considerable plastic deformation (figure S3a) are compared to ones with only viscoleastic deformation (figure S3b). The former were used to extract hardness and reduced elastic modulus in an Oliver and Pharr like approach[8,9]. The latter are the basis for the measurement of viscoelastic properties as described in the main text. Please note that not the force vs. indentation depth plots are fitted to a viscoelastic model but the creep curves (indentation depth vs. time), as is described in the main text.

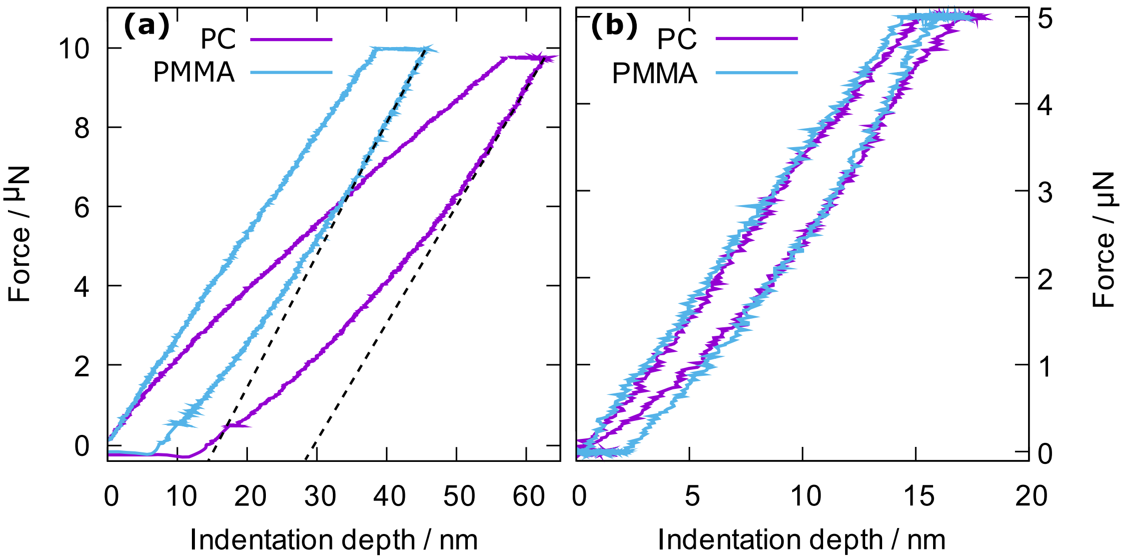


Figure S3: Force vs. indentation depth plots of (a) AFM based nanoindentation with considerable plastic deformation and (b) AFM-NI to measure viscoelasticity. The dashed lines in (a) represent the unloading slopes which are related to the elastic modulus. Please note the differently scaled axes in (a) and (b).

By comparing figures S3a and b it becomes obvious that the curves recorded with only viscoelastic deformation present, appear to be much more influenced by noise. The reason for this is that the curves in figure S3a are recorded with a much larger maximum indentation depth (between 30 nm and 60 nm) compared to figure S3b (maximum indentation depth $< 20$ nm). This demonstrates that allowing larger deformations could be an alternative way to reduce the scattering of the recorded curves, instead of averaging them. However, a disadvantage of this approach is that tips with larger radius and stiffer cantilevers would be needed to keep the strain low and provide the ability to generate the necessary forces.

## Bibliography


[1] K. L. Johnson, K. Kendall and A. D. Roberts, *P. Roy. Soc. Lond. A: Mat.*, 1971, **324**, 301–313.

[2] E. Barthel, *J. Phys. D: Appl. Phys.*, 2008, **41**, 163001.

[3] V. L. Popov, in *Contact Mechanics and Friction: Physical Principles and Applications*, Springer Berlin Heidelberg, Berlin, Heidelberg, 2010, ch. Rigorous Treatment of Contact Problems – Adhesive Contact, pp. 71–79.

[4] D. Tabor, *Rev. Phys. Technol.*, 1970, **1**, 145–179.

[5] S. Basu, A. Moseson and M. W. Barsoum, *J. Mater. Res.*, 2006, **21**, 2628–2637.

[6] S. Pathak, S. R. Kalidindi, C. Klemenz and N. Orlovskaya, *J. Eur. Ceram. Soc.*, 2008, **28**, 2213–2220.

[7] S. R. Kalidindi and S. Pathak, *Acta Mater.*, 2008, **56**, 3523–3532.

[8] W. C. Oliver and G. M. Pharr, *J. Mater. Res.*, 1992, **7**, 1564–1583.

[9] C. Ganser, U. Hirn, S. Rohm, R. Schennach and C. Teichert, *Holzforschung*, 2014, **68**, 53–60.